**Synthesis of 4-Chloro-1,3-Diazobenzene Bent-Core Liquid Crystals and Characterizations of Their Mesogenic Behavior and Photosensitivity**

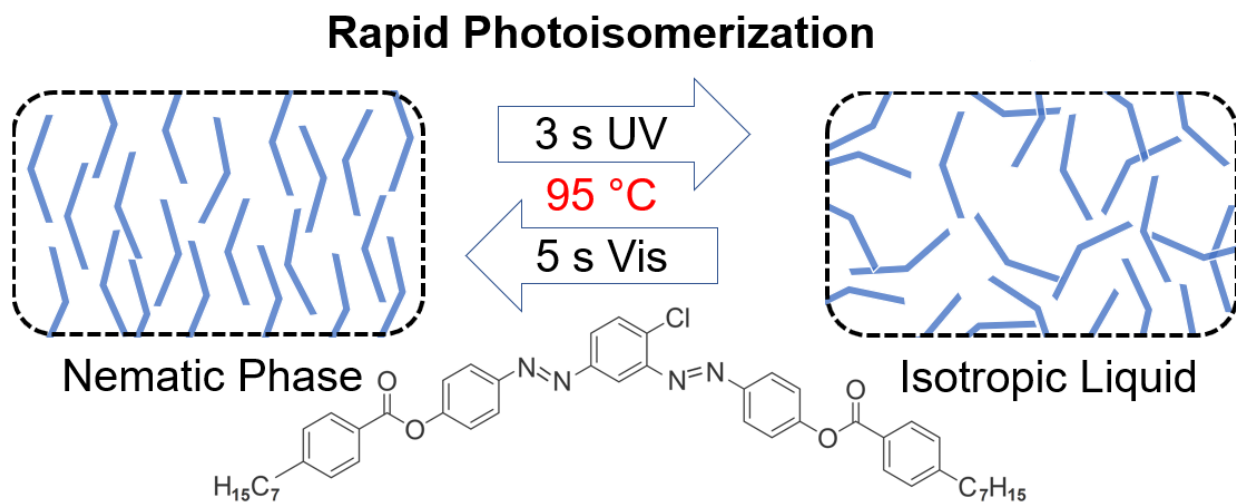Zelong Zhang[a*], Jinying Lu[b], Daoren Yan[b], Zhiyong Zhang[b*], Jintao Guan[b], and Junfei Qiao[b]

[a]Department of Geology and Geophysics, Louisiana State University, Baton Rouge, LA, USA

[b]Department of Chemistry and Environmental Engineering, Wuhan Polytechnic University, Wuhan, China

Corresponding authors*

Zelong Zhang zelongz@lsu.edu

Zhiyong Zhang zzy6211@126.com

**Graphical Abstract**

**Abstract**

16

17        Azobenzene-based bent-core liquid crystals demonstrate a variety of mesomorphic

18 behaviors and photochromic properties which are desirable for optical switching. In this study, a

19 series of novel compounds were synthesized by adding azo functional groups and chlorine

20 substituent to the central bent-cores to form a 4-chloro-1,3-dizaophenylene bent-core. Fourier-

21 transform infrared spectroscopy (FTIR), $^1$H and $^{13}$C nuclear magnetic resonance (NMR), mass

22 spectrometry (MS), differential scanning calorimetry (DSC), polarized optical microscopy (POM),

23 and ultraviolet–visible spectroscopy (UV-Vis) were performed to evaluate the structure, mesogenic

24 properties, and photosensitivity of these synthesized compounds. The experimental results show

25 that these compounds exhibit a broad temperature window up to 63.8 °C for nematic phase. In

26 addition, the enhancement of photonic properties of these compounds was exemplified by the high

27 conversion ratio and the rapid rate of *trans – cis* photoisomerization of compound **4c**. The *cis*

28 fraction of **4c** can reach 0.81. At 95 °C, **4c** in nematic phase became isotropic liquid under UV-

29 irradiation in 3 seconds and can be restored to nematic under natural visible light in 5 seconds. At

30 room temperature, **4c** when dissolved in ethyl acetate solution can reach photostationary state in

31 10 seconds. Quantum mechanics modeling confirms that using azos instead of esters as the central

32 linkages can effectively reduce the molecular dipole moment, which appears to promote favorable

33 mesogenic behaviors and photonic characteristics. Moreover, varying the carbon number in the

34 terminal alkyl chains can alter molecular dipole, especially the polarizability anisotropy, of which

35 the variation is strongly correlated with the phase transition temperature and temperature range of

36 nematic phase. These findings suggest that 1) changing azo group position can effectively alter the

37 molecular dipole; 2) reducing molecular dipole interaction can promote favorable photonic

38 properties of azobenzene bent-core liquid crystal. This study linking the mechanistic details with

39   mesogenic behaviors provides a novel approach to improve the material design for photonic

40   applications.

41   Keywords:

42   bent-core liquid crystal; 4-chloro-1,3-diazobenzene; synthesis; nematic phase; photoisomerization;

43   quantum mechanics calculation;

44

45

## 1. Introduction

Signal switch is vital to the data transmission in communication and information technology. Photonic technology such as optical fiber has tremendous bandwidth compared to electrical technology because of the significantly weaker interactions between photons than that of electrons.[1] However, current design of optical switch still requires electrical control due to the limitation of materials, which hinders the deployment of photonic technology to a larger scale. Therefore, discovering new phototunable materials is critical to the future design of optical switch.[1–3]

Photosensitive liquid crystals, especially azobenzene-based bent-core liquid crystals (ABLCs), are promising materials for optical switching.[4–7] ABLC compounds can be highly photochromic and mesogenic due to the reversible *trans-cis* photoisomerization of azo group (–N=N–) induced by proper irradiation of ultraviolet or visible light.[8,9] These characteristics also give rise to a myriad of potential applications of ABLC in areas such as elastomer, holographic imaging, optical data storage, and nanomachines.[10–14]

To date, the majority of ABLC compounds implemented at least one ester as the direct linkage of the central bent-core and or deployed azo groups in the distant side arms,[8,15–20] which usually exhibited high temperatures of phase transition, far above room temperature 25 °C, and narrow temperature ranges of nematic phases. To lower the phase transition temperature and broaden the temperature range of nematic phases, recent studies emphasized on structural alterations such as introducing different lateral substitutions on the bending core,[15,16,21] adjusting the number of aromatic units,[17,22–24] modifying the type, number, and position of linkage groups,[17,25–28] and changing the type and length of the terminal chains.[17,18,28–30] Yet, the mesogenic phase behaviors of current ABLCs are still unfavorable for practical applications.

We hypothesized that the linking groups adjacent to the central bent-core play a vital role in determining the mesogenic properties of ABLCs. The ester groups commonly used on the central bent-cores as the linking units can induce strong electrostatic forces that contribute to the intermolecular interactions of ABLCs, leading to high phase transition temperatures and narrow nematic phases. Previous studies suggest that the location of azo linkage does not exert significant influence on the mesogenic behavior; if azo bond is close to central ring, it can even inhibit the formation of mesogenic phases.[17,25] However, their conclusions were based on compounds with a single azo linkage. This study proposed an alternative approach to improve the design of ABLC by using two azo bonds instead of esters as the central linkages that connect the central bent-core, which would weaken the intermolecular interactions and therefore enhance the overall performance of ABLC. ABLC compounds synthesized in this study were derived from 4-chloro-1,3-diazobenzene. Each of them possesses two azo linkages and one chlorine substituent in the 1,3-position and 4-position, respectively, at the central aromatic ring and terminal alkyl chains.

**2. Materials and methods**

*2.1 Materials*

Anhydrous aluminum trichloride (chemically pure), N, N'-dicyclohexylcarbodiimide (DCC), and 4-dimethylaminopyridine (DMAP) were obtained from Tianjin Fuchen Chemical Reagent (China), Nanjing Chemical Reagent (China), and Xiya Reagent (China), respectively. All chemicals used in this study are of analytical grade, unless otherwise stated. 4-n-hexylbenzoic acid, 4-n-heptylbenzoic acid, 4-n-octylbenzoic acid, 4-n-decylbenzoic acid, and 4-n-decylbenzoic acid were synthesized in our laboratory. Reaction products were purified by silica gel column chromatography and recrystallized three times from ethanol – dichloromethane 1:1 mixture.

### 2.2 Characterization

Reactions required low temperature were conducted in Zhengzhou Greatwall DHJF-8002 low temperature constant temperature stirring reaction bath. Infrared spectroscopy was performed by a Thermo Nicolet Avatar 330 FTIR. $^1$H NMR spectra were obtained from a Varian INOVA 400 spectrometer (400 MHz) using tetramethylsilane (TMS) as the reference standard. Differential scanning calorimetry (DSC) experiments were conducted on a TA Instruments DSC Q-20 with a scanning rate of 5 °C/ min and natural cooling. Phase transition and optical textures of liquid crystal compounds were characterized by a polarizing optical microscope (POM) XPN-100E from Shanghai Changfang Optical Instrument.

UV-Visible absorption spectroscopy was collected by a UV-8000S spectrophotometer from Shanghai Metash Instrument. UV-Vis experiments were conducted using a wavelength range from 200 nm to 550 nm and a scan rate of 1 nm/s. UV-Vis spectral data were used i. to measure the isomer fraction by dissolving sample in dilute solution of ethyl acetate ($2.5 \times 10^{-5}$ mol/L) at room temperature and ii. to characterize the UV-induced photoisomerization of mesogenic phases at 95 – 100 °C. The data collection of UV-Vis spectroscopy started when the absorbance value of the two consecutive measurements were identical.

### 2.3 Synthesis

Compound **4a–4g** were synthesized according to Figure 1, of which the steps are described below.

#### 2.3.1 Synthesis of 4-chloro-1,3-dinitrobenzene (I)[31]

Chlorobenzene (40 ml) was added into a 500 ml three-neck flask with magnetic stir bar. The temperature was maintained at 95 °C. Concentrated nitric acid (117.6 ml) and concentrated

sulfuric acid (123.6 ml) were added in the flask. The solution mixture was stirred for 5 hours, in which the reaction was monitored by thin layer chromatography (TLC). The reaction product was washed with hot water to reach pH neutral, vacuum-filtered, and air-dried. This step produced yellow crystals.

Yield: 55.07 g, 85.2%, melting point (m.p.) 48 °C. FTIR (KBr, $v_{max}$, cm$^{-1}$): 3082.32 (Ar–H), 1618.15, 1528.35 (Ar), 1474.40, 1352.32, 1306.78, 1202.84, 1102.45.

*2.3.2. Synthesis of 4-chlorom-1,3-diaminobenzene* **(II)**[32]

pure iron powder (28 g, 0.5 mol), glacial acetic acid (45 g), and 100 mL deionized water were added into a 250 mL three-necked flask. Once the solution was heated to 70 ~ 80 °C, compound **(I)** (20.2 g, 0.1 mol) was added. The reaction was carried out for 4h, which was monitored by TLC to ensure completion. The product mixture was filtered and washed with hot water twice to remove nonpolar impurities. The pH of the filtrate was adjusted to pH 10.0 with saturated $Na_2CO_3$ solution. The organic phase was extracted with 30 mL ethyl acetate repeated for thrice and then dried with anhydrous $K_2CO_3$, yielding a crude black product. The product was purified by silica gel column chromatography. This step produced a needle-shaped brown solid of compound **(II)**.

Yield: 10.5 g, 74.2%, m.p. 86-88 °C. FTIR (KBr, $v_{max}$, cm$^{-1}$): 3343.37, 3405.11, 3315.06 (N–H), 3211.17 (Ar–H), 1615.53, 1577.97, 1496.67, 1451.98 (Ar), 1333.37, 1274.30, 1208.48, 1147.56, 1106.67, 1044.15, 845.96.

*2.3.3 Synthesis of 4-chloro-1,3-bis (4-hydroxyphenyl)azobenzene* **(III)**[33]

Chilled concentrated hydrochloric acid (40 mL, 0.5mol) was added in a three-necked flask. The temperature was maintained at below –25 °C. A solution prepared from sodium nitrite (12.5

g, 0.18 mol) and 19 mL deionized water was added dropwise while stirring slowly. Then, a solution prepared from compound (**II**) (7.15g, 0.05mol) and concentrated hydrochloric acid (25mL) was added in multiple steps while gradually increasing the stirring speed. The reaction lasted for 0.5 hour, generating a yellow transparent liquid. Urea pellets (4.8 g, 0.08mol) were added into the liquid dropwise while stirring to yield a diazonium salt.

The diazonium salt was added slowly to a three-necked flask containing a solution of phenol (11.3g, 0.12mol), sodium carbonate (31.8g, 0.3mol) and water (200ml). The mixture in the flask was stirred for 3h in a cold-water bath, of which the reaction was monitored by the TLC. Once the reaction was completed, the mixture was filtered. The resultant filter cake was recrystallized from ethanol. 10.96g of yellow crystals of compound (**III**) was obtained. Yield: 62.3%. m.p. 164 ~ 166 °C. FTIR (KBr, $\nu_{max}$, cm$^{-1}$): 3333.1 (–OH), 1702.11, 1583.27, 1502.13, 1473.53 (Ar), 1256.44, 1223.10, 1192.22, 1069.13, 1028.42, 853.33; $^1$H NMR (400 MHz, CDCl$_3$, δ, ppm): 8.31 (s, 1H), 7.95 ~ 7.97 (d, J = 8 Hz, 1H), 7.67 ~ 7.77 (m, 5H), 7.18 ~ 7.21 (t, J = 6 Hz, 4H), 5.08 (s, 2H); $^{13}$C NMR (100 MHz, CDCl$_3$): 161.118, 152.732, 149.855, 130.145, 129.282, 124.259, 120.387, 118.365, 115.927. MS m/z (%): 353.65 (65.5, M+1), 231.67 (19.5), 111.67 (13.1).

*2.3.4 Synthesis of ABLC compound* **4c**[34]

Compound (**II**) (1.66 g, 5mmol), 4-alkylbenzoic acid (10mmol), DCC (12 mmol), DMAP (1.2 mmol) and CH$_2$Cl$_2$ (50mL) were added into a 100 mL three-necked flask. The mixture was stirred at room temperature for 24 hours, and the reaction was monitored by TLC. Upon completion, the mixture was filtered and washed with CH$_2$Cl$_2$. The solute was extracted by evaporating the solvent under reduced pressure and then purified by silica gel column chromatography.

158    4-Chloro-1,3-bis(4-((4-heptylphenyl)acyloxy)-1-(E)-azophenyl)benzene **4c**: 2.48g yellow

159    needle crystal, yield: 71.5%, m.p. 84 ~ 85.5 °C. FTIR (KBr, $v_{max}$, cm$^{-1}$): 2918.17, 2849.16 (–CH2),

160    1169.63, 1645.76, 1613.79, 1542.68, 1507.81, 1450.59 (Ar), 1355.50, 1339.12, 1296.69, 1233.43,

161    1125.32, 841.01. $^1$H NMR (400 MHz, CDCl$_3$) δ (ppm): 8.32 (s, 1H), 8.09 ~ 8.11 ( d, J = 6.5 Hz,

162    4H), 7.99 ~ 8.01 (d, J = 8 Hz, 4H), 7.53 ~ 7.55 (t,  J = 6.5 Hz, 1H), 7.18 ~ 7.20 (d, J = 8 Hz, 4H),

163    7.07 ~ 7.09 (d, J = 6.0 Hz, 4H), 2.60 ~ 2.63 (t, J = 6 Hz, 4H), 1.63 ~ 1.66 (m, 4H), 1.31 ~ 1.36 (m,

164    16H), 0.89 ~ 0.92 (t, J = 6 Hz, 6H). $^{13}$C NMR (100 MHz, CDCl$_3$) δ (ppm): 164.819, 152.378,

165    152.352,  150.212,149.701,  130.321,  129.732,  128.715,  126.590,  125.356,  124.289,  122.425,

166    116.423, 36.222, 31.852, 31.225, 30.285, 29.285, 22.589, 14.152. MS m/z (%): 757.59 (71.10，

167    M+1), 587.70 (16.5), 295.58 (28.1).

168    *2.3.4 Computational Simulations*

169    At the molecular scale, phase transition is the rearrangement of molecules. Phase

170    transitions of nematic liquid crystals are intrinsically associated with the intermolecular

171    interactions especially the long-range non-bonded electrostatic interactions.[35–40] Therefore, it is

172    necessary to examine the molecular polarity that determine the intermolecular electrostatic

173    interactions.[37,41,42] The degree of molecular polarity can be assessed by measuring molecular

174    dipole moment and molecular polarizability.[37,41,42] In this study, computational simulations were

175    performed to determine the molecular properties.

176    Before characterizing the molecular properties, the optimal molecular geometry of each

177    compound needs to be identified at the ground state. Each compound exhibit numerous conformers.

178    For example, compound **4c** contains 104 atoms and 10 rotatable bonds, which generates

179    approximate 60,000 conformers. Apparently, searching conformers of global energy minimum is

180 not viable for computationally demanding simulations especially for those based on quantum

181 mechanics. Therefore, molecular dynamic simulation was applied to screen candidate conformers

182 of global energy minimum. After the screening, quantum mechanics techniques were carried out

183 on the selected conformers to finalize the geometry optimization. All molecular properties were

184 obtained based on the optimized molecular geometry.

185 Specifically, molecular dynamics (MD) simulations were conducted by Avogadro 1.2.0, a

186 free cross-platform program. General Amber force field was used due to its specific

187 parameterization for organic molecules.[43–46] Geometry optimization was performed using steepest

188 descent algorithm with a convergence energy of $10^{-7}$ kcal/mol. Input structural parameters of

189 azobenzene moiety were adopted from previous density functional theory calculation and X-ray

190 diffraction data.[47,48] To find the candidate conformers of the global energy minimum, systematic

191 rotor search was carried out. Semi-empirical (SE) quantum chemistry calculations were performed

192 by MOPAC (Molecular Orbital PACkage, 2016), a general-purpose semi-empirical molecular

193 orbital package free for academic and not-for-profit use, using PM7 Hamiltonian and Baker's

194 EigenFollowing method.[49,50]

195 To elucidate the dynamics of intermolecular interactions, molecular dipole moment and

196 molecular polarizability were calculated.[51,52] Frequency-dependent dynamic polarizabilities were

197 calculated by time-dependent Hartree-Fock theory.[53] Due to the complexity to express

198 polarizability, here we only compared measurements of polarizability at zero frequency (0 eV)

199 including polarizability isotropic average ($\alpha_{iso}$) and polarizability anisotropy ($\Delta\alpha$). They can be

200 derived by

201
$$\alpha_{iso} = \frac{\alpha_{xx} + \alpha_{yy} + \alpha_{zz}}{3}$$

202     and

203
$$\Delta\alpha = \sqrt{\frac{(\alpha_{xx} - \alpha_{yy})^2 + (\alpha_{yy} - \alpha_{zz})^2 + (\alpha_{zz} - \alpha_{xx})^2}{2}}$$

204     where $\alpha_{ii}$ is the principal component of polarizability along the $i$th axis.[52,54,55] The components of

205     dipole moment and polarizability are listed in Table S1 and S2, respectively. In addition, density

206     functional theory (DFT) calculations were deployed to demonstrate that its results are comparable

207     to those of SE (technical details in supplement text). The molecular dipole moments of compounds

208     **4a-4g** calculated by MD, SE, and DFT are compared in Figure S1 and Table S1.  Moreover, to

209     compare the experimental results, simulated UV-Vis spectra of **4c** *trans* and *cis* were obtained by

210     DFT as shown in Figure S2, which indicates that the *trans* and *cis* configurations of **4c** are

211     reasonably modelled in our study.

212     **3. Results**

213     *3.1 Phases transition temperatures and enthalpies of compounds* **4a–4g**

214          The phases, transition temperatures, and transition enthalpies of compounds **4a–4g** are

215     listed in Figure 2 – 3 and Table 1. DSC analysis in Figure 2 shows that while increasing temperature

216     all compounds **4a–4g** displayed an array of phases, including crystalline solid (Cr), smectic (Sm),

217     nematic (N), and isotropic liquid (Iso). The temperatures of phase transition are ranging from

218     65.92 °C to 103.37 °C for Cr – Sm, 91.36 °C to 124.36 °C for Sm – N, and 131.26 °C to 162.36 °C

219     for N – Iso. Figure 3 shows that the enthalpies for Cr – Sm, Sm – N, and N – Iso transitions are

220     ranging from 30.3 kJ/mol to 52.3 kJ/mol, 7.4 kJ/mol to 19 kJ/mol, and 2.6 kJ/mol to 4.7 kJ/mol,

221     respectively.

222          The terminal chain length (carbon number, $n$) demonstrates a pronounced and systematic

223  effect on the phase transition of **4a–4g**. Overall, as the carbon number (n) in the terminal alkyl

224  chains increases, the phase transition temperatures decrease except for the Sm – N transition and

225  transition enthalpies increases except for the N – Iso transition. However, the temperatures of Sm

226  – N transition initially decreased and then increased as the carbon number increased. The impact

227  from carbon number to the N – Iso transition enthalpies was insubstantial.

228         In particular, Figure 2 shows that generally the phase transition temperatures decrease over

229  the increment of carbon number (*n*) in the terminal alkyl chains. Notably, the phase transition

230  temperatures of N – Iso exhibited a linear relationship with respect to the carbon number, giving a

231  linear fitting with a $R^2$ (the coefficient of determination) of 0.96. A similar trend was also found

232  for the phase transition of Cr – Sm, which gives a $R^2$ of 0.96 if treating the data of compound **4g**

233  as an outlier. However, the linear relationship between the Sm – N transition temperatures and the

234  carbon number is insubstantial with a $R^2$ of 0.01, which indicates the phase behaviors in Sm – N

235  transition are inconsistent with those in the other phase transitions. The only structural difference

236  between compounds **4a–4g** is the length of terminal alkyl chain. Therefore, the inconsistent

237  changes in phase behavior during Sm – N transition could be attributed to the structural difference

238  associated with the terminal chains of compound **4a–4g** during this phase transition.

239         Additionally, as shown in Figure 2 and Table 1, the liquid crystal phases transition

240  temperature of compound **4a–4g** generally exhibited wide temperature windows of both

241  mesogenic phases ranging from 58.99 °C to 70.68 °C and nematic phases ranging from 19.89 °C

242  to 63.84 °C. In particular, the widest temperature window of mesogenic phase (70.68 °C) and

243  nematic phase (63.84 °C) were both exhibited by compound **4c**, which possessed a moderate length

244  of terminal chains (*n* = 7). The narrowest temperature window for nematic phase (19.8 °C) was

245  exhibited by compound **4f**, which also exhibited the lowest melting point 65.9 °C.

246      A previous study showed that the liquid crystal compounds can exhibit a systematic odd-

247     even periodic pattern on phase transition properties according to the carbon number in the terminal

248     alkyl chains.[56–60] Through closer examinations, we noticed that the changes in melting points,

249     clearing points, and enthalpies exhibit similar odd-even pattern as shown in Figure 2 and 3.

250     *3.2 Molecular dipole moments and polarizability of* **4a–4g**

251     The optimized geometries of **4a–4g** are illustrated in Figure 4, together with their dipole

252     moments. Table 2 list dipole moments ($\mu$), polarizability isotropic average ($\alpha_{iso}$), and polarizability

253     anisotropies ($\Delta\alpha$) of isomers of **4a–4g**. The $\mu$ ranges from 3.7 to 6.1 Debye for *trans* and 4.4 to 9.1

254     Debye for *cis* isomers, respectively. The $\alpha_{iso}$ ranges from 86.8 to 111.4 Å$^3$ for trans and 82.9 to

255     108.4 Å$^3$ for cis, respectively. The $\Delta\alpha$ ranges from 20.6 to 31.0 Å$^3$ for *trans* isomers and 9.8 to

256     18.7 Å$^3$ for *cis* isomers, respectively. Figure 5 plots the $\mu$, $\alpha_{iso}$, and $\Delta\alpha$ against the carbon number

257     ($n$) of the terminal chains, which shows clear trends: i) the variances in molecular dipole between

258     *trans* and *cis* isomers: minimal when $n = 7$ and maximum when $n = 12$; ii) increasing carbon

259     number $n$ can linearly increase the $\alpha_{iso}$ for both *trans* and *cis* with the same rate; iii) for *trans*, the

260     increment in $n$ initially reduces the $\Delta\alpha$ when $n$ in the range of 5 to 7 and then gradually increases

261     the $\Delta\alpha$ in the $n$ range of 8 to 12., whereas the *cis* isomers show no clear trend of $\Delta\alpha$.

262     *3.3 Photosensitivity measurement, using* **4c** *as an example*

263     Photosensitivity was measured by UV-Vis spectroscopy. As shown in Figure 6, a series of

264     UV-Vis spectra of **4c** (dissolved in ethyl acetate, room temperature) was collected under the UV

265     irradiation (365 nm, 1 mW/cm$^2$) for 2 s, 5 s, 10 s, and 30 s. All these spectra exhibited a similar

266     pattern: a strong band and a weak band in the regions of 330 – 340 nm and 430 – 450 nm,

267     respectively. The strong band is attributed by the $\pi$–$\pi$* transition of the azo unit, which indicates

268    the presence of *trans* isomer, while the weak band is ascribed to the *cis* n–π* transition in cis

269    isomer.[8] As the UV irradiation time prolonged, the intensity of the strong band decreased rapidly,

270    whereas the signal of the weak band gradually increased. This pattern indicates the occurrence of

271    *trans* → *cis* photoisomerization.[8] Interestingly, dissolved **4c** reached photostationary state in 10

272    seconds, significantly faster than reported response rates of similar ABLCs, which are in minutes

273    and even hours.[14,16,17,19–21,25,27,61–64]

274         As shown in Figure 6 (bottom 3 insets), compound **4c** can turn from crystalline solid into

275    nematic phase by heating the pure sample to 95 °C. Under the UV irradiation (365 nm, 1 nW/cm$^2$),

276    nematic **4c** became isotropic liquid in 3 seconds. Without the UV irradiation, **4c** restored to nematic

277    phase within 5 seconds under indoor natural visible light. These phenomena indicate the presence

278    of reversible *trans* – *cis* photoisomerization. The UV-induced *cis* isomers destabilized the orderly

279    arrangement of *trans* isomers in nematic phase and possibly reduced the phase transition

280    temperatures.[4,27] Under visible light, the backward *trans* ← *cis* photoisomerization started and

281    restored the nematic phase of ***4c***. A video of the phase transitions under POM is available in

282    supplement (POM_UV.mp4).

283         The ratio of the isomer concentrations can be estimated by the following equation:

284    $$[cis]_t \, / \, [trans]_0 = (1 - A_t \, / \, A_0) \, / \, (1 - \varepsilon_{cis} \, / \, \varepsilon_{trans})^{[65,66]}$$

285    where $[cis]_t$ is the concentration of *cis* isomer at time $t$, $[trans]_0$ the initial concentration of *trans*

286    isomer, $A_0$ and $A_t$ are the absorbances at the wavelength of the same chromophore of sample

287    compound, in which all sample compounds in solution are either *trans* or *cis* isomers, $\varepsilon_{cis}$ and $\varepsilon_{trans}$

288    the molar attenuation coefficients (also known as molar extinction coefficient and molar absorption

289    coefficient) of the *cis* and *trans* isomers at a given wavelength of light, respectively.[66]

290        Previous studies on similar azobenzene-based compounds report $\varepsilon_{cis} / \varepsilon_{trans}$ ratios of 0.050,

291    0.053, 0.055, 0.056, and 0.05, corresponding to the UV wavelengths of 320 nm,[66] 325 nm,[66] 355

292    nm,[67] 369.5 nm,[68] and 370 nm,[69] respectively. Therefore, we selected 0.05 as the $\varepsilon_{cis} / \varepsilon_{trans}$ ratio

293    to estimate the isomer fraction under the irradiation of 365 nm UV. The strong absorption band at

294    334 nm collected from the 30-second UV irradiation test generated a $A_t / A_0$ ratio of 0.2348, giving

295    a $[cis]_t / [trans]_0$ ratio of 0.81. This ratio indicates that 81% of nematic **4c** had converted from *trans*

296    to *cis* isomers, which is one of the highest among the reported ratios of similar azobenzene-based

297    compounds.[3,67–72]

## 298    4. Discussion

### 299    *4.1 Effect of azo position*

300        To examining the effect of azo position on ABLC, molecular properties of **4c** and its

301    counterpart **4c-c** using two esters as central linkages were calculated and compared as shown in

302    Figure 7 and Table 3. The comparison shows that the dipole moments of *trans* **4c** (3.85 D) is

303    significantly smaller than that of **4c-c** (6.95 D). The dipole moment of *cis* **4c** (4.11 D) is also

304    noticeably smaller than that of **4c-c** (5.04 D). Interestingly, the DFT calculation shows a larger

305    dipole moment of *cis* **4c** than that of *cis* **4c-c**. Nevertheless, small dipole moment indicates weak

306    electrostatic interactions. The small dipole moment of phase of *trans* **4c** leads to the low melting

307    point and wide temperature windows of nematic phase. In addition, the molecular structures of **4c**

308    isomers prone to form an orderly geometry likely due to the small molecular structures attaching

309    to the rotatable ester bonds. Therefore, applying azo group as the central linkage to the bent core

310    can lower the melting point and broaden the temperature windows of mesogenic phases.

311        Moreover, the polarizabilities of *trans* and *cis* of **4c** are noticeably higher than those of **4c-**

312 **c**, which corroborates the experimental observations that **4c** is superior to its counterpart **4c-c** in

313 terms of *trans – cis* photoisomerization rates as shown in Table 3. At zero frequency (0 eV), both

314 the $\alpha_{iso}$ and $\Delta\alpha$ of *trans* **4c** (93.6 and 20.7 Å$^3$) are larger than 92.0 and 16.5 Å$^3$ of *trans* **4c-c**,

315 respectively. Since the polarizability $\alpha$ is the first-order response coefficient of molecular

316 polarization, higher $\alpha$ value typically leads to higher extent of molecular polarization.[51] Dipole

317 moment can drive molecules or molecular groups into favorable orientations, promoting the

318 formation of new phase.[40] The difference in $\alpha$ may also be reflected in dipolar moment and

319 therefore in phase transition rate. Thus, it is possible that the high polarizability can lead to a rapid

320 phase transition as well as a high *trans – cis* photoisomerization rate as demonstrated by compound

321 **4c**. Further investigation is required to quantify the impact of molecular polarizability on phase

322 transition behavior.

### *4.2 Effect of molecular dipole on phase transition behaviors*

324       Figure 5 (bottom right inset) compares Sm – N transition temperatures and temperature

325 ranges of nematic phase of **4a–4g** compounds with their corresponding dipole moments and

326 polarizability anisotropies. This comparison shows that the impact from terminal chain length to

327 the $\mu$ and $\Delta\alpha$ remarkably resembles that of the phase transition temperatures of Sm – N, whereas

328 the effect of terminal chains on the temperature ranges of nematic phase appears to be the opposite.

329 Notably, among these compounds, **4c** exhibits the smallest dipole moment, the lowest temperature

330 of Sm – N phase transition, and the widest range of nematic phase. These patterns show that the

331 molecular polarization can indicate the degree of intermolecular interactions in nematic phase,

332 which implies that the nematic phase is the domain of the long-range electrostatic interactions. In

333 addition, an apparent odd-even periodic pattern of dipole moments with respect to the carbon

334 number was observed, which is consistent with our measurements of the phase transition properties.

335      Figure 4 shows that varying the length of terminal alkyl chains has no apparent impact on

336    the structure of central units with five aromatic rings but causes substantial changes to the

337    structures of terminal alkyl chains. As the carbon number increases, the terminal chains become

338    curly and formed a 'U' shape when the terminal chain has more than nine carbon atoms. This

339    observation suggests that increasing the carbon number can promote the structural disorder of

340    terminal alkyl chains and therefore enhance the molecular dipole moment. Combining the

341    information of $\mu$, $\Delta\alpha$ , and the molecular geometry (Figure 4 and 5), it appears that effect of

342    terminal alkyl chain is biphasic. Elongating the alkyl chains can reduce both $\mu$ and $\Delta\alpha$ and improve

343    the flexibility of terminal chain structures. However, when the terminal chains were long enough

344    ($n > 7$) that can induce structural disorder, $\mu$ and $\Delta\alpha$ would cease to decrease and may even increase

345    as the result of enhanced molecular asymmetry. Therefore, terminal alkyl chain can either enhance

346    or reduce the $\mu$ and $\Delta\alpha$ of ABLCs depending on the number of carbon atom, leading to a biphasic

347    effect on the behaviors of nematic phases.

348    **5. Conclusion**

349       To date, this is the first study to synthesize azobenzene-based bent-core liquid crystals

350    (ABLC) using two azo bonds as direct linkages of the central bent-core. A series of 4-chloro-1,3-

351    diazobenzene bent-core liquid crystal **4a–4g** were synthesized with different length of terminal

352    alkyl chains. These compounds compound exhibited broad temperature windows of nematic phase.

353    In addition, compound **4c** exhibited rapid *trans – cis* photoisomerization in few seconds.

354    Theoretical calculations, such as molecular dynamics (MD) and quantum mechanics (QM)

355    confirmed that when using two azo bonds as the linkage instead of two esters on the central bent-

356    core, the electrostatic interactions are substantially weakened and molecular polarizabilities are

357    enhanced. This finding indicates using azo bonds as central linkages can promote favorable phase

behaviors and optical properties. Molecular dipole moments calculated by both MD and QM are strongly correlated with the phase transition behavior such as temperatures of Sm – N phase transition and temperature windows of nematic phase. This correlation suggests that electrostatic interactions are the main contributor of intermolecular interactions, especially in nematic phases. According to the simulation results, the terminal alkyl chains demonstrate a diphasic effect on the molecular dipole due to the structural disorder of overextended alkyl chain, which is consistent with the nematic phase behavior of ABLC.

In summary, this study proposed a novel method to synthesize photosensitive liquid crystal compound and deployed synergistic approach to elucidate material properties. Such efforts are imperative for advancing future design of azobenzene-based bent-core liquid crystals:

1.  Using 1,3-diazobenzene as the bent-core can substantially reduce the phase transition temperature and achieve photoisomerization rate (*trans – cis* photoisomerization in seconds with 80% conversion)
2.  Changing carbon number of alkyl chain exerts a biphasic effect on the molecular polarization and phase behavior.
3.  Molecular dipole and polarizability anisotropy appear to be strongly correlated with phase behavior properties such as Sm – N phase transition temperature and temperature window of N phase. Altering molecular polarity through carbon number of terminal chains is a promising approach to design novel ABLC compounds.

**Acknowledgments**

380    11074054 and 11374067.

381    **Disclosure statement**

383    **ORCID**

384    Z. Zhang http://orcid.org/0000-0002-0807-8991

385

386

**Disclosure statement**

No potential conflict of interest was reported by the authors.

**ORCID**

Z. Zhang http://orcid.org/0000-0002-0807-8991

## References

(1)     *Optical Switching*; El-Bawab, T. S., Ed.; Springer US: Boston, MA, 2006. https://doi.org/10.1007/0-387-29159-8.

(2)     De Sio, L.; Ricciardi, L.; Serak, S.; La Deda, M.; Tabiryan, N.; Umeton, C. Photo-Sensitive Liquid Crystals for Optically Controlled Diffraction Gratings. *J. Mater. Chem.* **2012**, *22* (14), 6669. https://doi.org/10.1039/c2jm16077c.

(3)     Aronzon, D.; Levy, E. P.; Collings, P. J.; Chanishvili, A.; Chilaya, G.; Petriashvili, G. Trans–Cis Isomerization of an Azoxybenzene Liquid Crystal. *Liquid Crystals* **2007**, *34* (6), 707–718. https://doi.org/10.1080/02678290701267480.

(4)     Ikeda, T.; Tsutsumi, O. Optical Switching and Image Storage by Means of Azobenzene Liquid-Crystal Films. *Science* **1995**, *268* (5219), 1873–1875. https://doi.org/10.1126/science.268.5219.1873.

(5)     Finkelmann, H.; Nishikawa, E.; Pereira, G. G.; Warner, M. A New Opto-Mechanical Effect in Solids. *Phys. Rev. Lett.* **2001**, *87* (1), 015501. https://doi.org/10.1103/PhysRevLett.87.015501.

(6)     Reddy, R. A.; Tschierske, C. Bent-Core Liquid Crystals: Polar Order, Superstructural Chirality and Spontaneous Desymmetrisation in Soft Matter Systems. *J. Mater. Chem.* **2006**, *16* (10), 907–961. https://doi.org/10.1039/B504400F.

(7)     Mahimwalla, Z.; Yager, K. G.; Mamiya, J.; Shishido, A.; Priimagi, A.; Barrett, C. J. Azobenzene Photomechanics: Prospects and Potential Applications. *Polym. Bull.* **2012**, *69* (8), 967–1006. https://doi.org/10.1007/s00289-012-0792-0.

(8)     Alaasar, M. Azobenzene-Containing Bent-Core Liquid Crystals: An Overview. *Liquid Crystals* **2016**, *43* (13–15), 2208–2243. https://doi.org/10.1080/02678292.2016.1175676.

(9)     Merino, E.; Ribagorda, M. Control over Molecular Motion Using the *Cis – Trans* Photoisomerization of the Azo Group. *Beilstein J. Org. Chem.* **2012**, *8*, 1071–1090. https://doi.org/10.3762/bjoc.8.119.

(10)    Natansohn, A.; Rochon, P. Photoinduced Motions in Azo-Containing Polymers. *Chem. Rev.* **2002**, *102* (11), 4139–4176. https://doi.org/10.1021/cr970155y.

(11)    Camacho-Lopez, M.; Finkelmann, H.; Palffy-Muhoray, P.; Shelley, M. Fast Liquid-Crystal Elastomer Swims into the Dark. *Nature Mater* **2004**, *3* (5), 307–310. https://doi.org/10.1038/nmat1118.

(12)    Wang, Y.; Li, Q. Light-Driven Chiral Molecular Switches or Motors in Liquid Crystals. *Adv. Mater.* **2012**, *24* (15), 1926–1945. https://doi.org/10.1002/adma.201200241.

(13)    Garcia-Amorós, J.; Reig, M.; Castro, M. C. R.; Cuadrado, A.; Raposo, M. M. M.; Velasco, D. Molecular Photo-Oscillators Based on Highly Accelerated Heterocyclic Azo Dyes in Nematic Liquid Crystals. *Chem. Commun.* **2014**, *50* (51), 6704–6706. https://doi.org/10.1039/C4CC01450B.

(14)    Sunil, B. N.; Srinatha, M. K.; Shanker, G.; Hegde, G.; Alaasar, M.; Tschierske, C. Effective Tuning of Optical Storage Devices Using Photosensitive Bent-Core Liquid Crystals. *Journal of Molecular Liquids* **2020**, *304*, 112719. https://doi.org/10.1016/j.molliq.2020.112719.

(15)    Rahman, M. L.; Asik, J.; Kumar, S.; Tschierske, C. Liquid Crystalline Banana-shaped Monomers Derived from 2,7-naphthalene: Synthesis and Properties. *Liquid Crystals* **2008**, *35* (11), 1263–1270. https://doi.org/10.1080/02678290802513808.

(16)    Lutfor, M. R.; Hegde, G.; Kumar, S.; Tschierske, C.; Chigrinov, V. G. Synthesis and Characterization of Bent-Shaped Azobenzene Monomers: Guest–Host Effects in Liquid Crystals with Azo Dyes for Optical Image Storage Devices. *Optical Materials* **2009**, *32* (1), 176–183. https://doi.org/10.1016/j.optmat.2009.07.006.

(17)    Nagaveni, N. G.; Raghuvanshi, P.; Roy, A.; Prasad, V. Azo-Functionalised Achiral Bent-Core Liquid Crystalline Materials: Effect of Presence of –N=N– Linkage at Different Locations in the Molecular Architecture. *Liquid Crystals* **2013**, *40* (9), 1238–1254. https://doi.org/10.1080/02678292.2013.805831.

(18)    Ghosh, S.; Begum, N.; Turlapati, S.; Roy, S. Kr.; Das, Abhijit. Kr.; Rao, N. V. S. Ferroelectric-like Switching in the Nematic Phase of Four-Ring Bent-Core Liquid Crystals. *J. Mater. Chem. C* **2014**, *2* (3), 425–431. https://doi.org/10.1039/C3TC31800A.

448  (19)  Paterson, D. A.; Xiang, J.; Singh, G.; Walker, R.; Agra-Kooijman, D. M.; Martínez-Felipe, A.; Gao, M.; Storey,
449        J. M. D.; Kumar, S.; Lavrentovich, O. D.; Imrie, C. T. Reversible Isothermal Twist–Bend Nematic–Nematic
450        Phase Transition Driven by the Photoisomerization of an Azobenzene-Based Nonsymmetric Liquid
451        Crystal Dimer. *J. Am. Chem. Soc.* **2016**, *138* (16), 5283–5289. https://doi.org/10.1021/jacs.5b13331.
452  (20)  Alaasar, M.; Poppe, S. Cybotactic Nematic Phases with Wide Ranges in Photoresponsive Polycatenars.
453        *Liquid Crystals* **2019**, 1–11. https://doi.org/10.1080/02678292.2019.1690062.
454  (21)  Alaasar, M.; Prehm, M.; Tschierske, C. Influence of Halogen Substituent on the Mesomorphic Properties
455        of Five-Ring Banana-Shaped Molecules with Azobenzene Wings. *Liquid Crystals* **2013**, *40* (5), 656–668.
456        https://doi.org/10.1080/02678292.2013.767949.
457  (22)  Horčic, M.; Kozmík, V.; Svoboda, J.; Novotná, V.; Pociecha, D. Transformation from a Rod-like to a Hockey-
458        Stick-like and Bent-Shaped Molecule in 3,4'-Disubstituted Azobenzene-Based Mesogens. *J. Mater. Chem.*
459        *C* **2013**, *1* (45), 7560. https://doi.org/10.1039/c3tc31593b.
460  (23)  Gimeno, N.; Pintre, I.; Martínez-Abadía, M.; Serrano, J. L.; Ros, M. B. Bent-Core Liquid Crystal Phases
461        Promoted by Azo-Containing Molecules: From Monomers to Side-Chain Polymers. *RSC Adv.* **2014**, *4* (38),
462        19694–19702. https://doi.org/10.1039/C4RA02079K.
463  (24)  Dingemans, T. J.; Murthy, N. S.; Samulski, E. T. Javelin-, Hockey Stick-, and Boomerang-Shaped Liquid
464        Crystals. Structural Variations on *p* -Quinquephenyl [†]. *J. Phys. Chem. B* **2001**, *105* (37), 8845–8860.
465        https://doi.org/10.1021/jp010869j.
466  (25)  Monika, M.; Prasad, V.; Nagaveni, N. G. Hockey Stick-Shaped Azo Compounds: Effect of Linkage Groups
467        and Their Direction of Linking on Mesomorphic Properties. *Liquid Crystals* **2015**, *42* (10), 1490–1505.
468        https://doi.org/10.1080/02678292.2015.1066889.
469  (26)  Bobrovsky, A.; Shibaev, V.; Hamplová, V.; Bubnov, A.; Novotná, V.; Kašpar, M.; Piryazev, A.; Anokhin, D.;
470        Ivanov, D. Photo-Optical Properties of Amorphous and Crystalline Films of Azobenzene-Containing
471        Photochromes with Bent-Shaped Molecular Structure. *Journal of Photochemistry and Photobiology A:*
472        *Chemistry* **2016**, *316*, 75–87. https://doi.org/10.1016/j.jphotochem.2015.10.021.
473  (27)  Alaasar, M.; Prehm, M.; Tschierske, C. Helical Nano-Crystallite (HNC) Phases: Chirality Synchronization
474        of Achiral Bent-Core Mesogens in a New Type of Dark Conglomerates. *Chem. Eur. J.* **2016**, *22* (19), 6583–
475        6597. https://doi.org/10.1002/chem.201505016.
476  (28)  Alaasar, M.; Prehm, M.; Brautzsch, M.; Tschierske, C. 4-Methylresorcinol Based Bent-Core Liquid Crystals
477        with Azobenzene Wings – a New Class of Compounds with Dark Conglomerate Phases. *J. Mater. Chem.*
478        *C* **2014**, *2* (28), 5487–5501. https://doi.org/10.1039/C4TC00533C.
479  (29)  Alaasar, M.; Prehm, M.; May, K.; Eremin, A.; Tschierske, C. 4-Cyanoresorcinol-Based Bent-Core Mesogens
480        with Azobenzene Wings: Emergence of Sterically Stabilized Polar Order in Liquid Crystalline Phases. *Adv.*
481        *Funct. Mater.* **2014**, *24* (12), 1703–1717. https://doi.org/10.1002/adfm.201302295.
482  (30)  Alaasar, M.; Prehm, M.; Brautzsch, M.; Tschierske, C. Dark Conglomerate Phases of Azobenzene Derived
483        Bent-Core Mesogens – Relationships between the Molecular Structure and Mirror Symmetry Breaking
484        in Soft Matter. *Soft Matter* **2014**, *10* (37), 7285–7296. https://doi.org/10.1039/C4SM01255K.
485  (31)  Yi, W.; Cai, C. Highly Efficient Dinitration of Aromatic Compounds in Fluorous Media Using Ytterbium
486        Perfluorooctanesulfonate and Perfluorooctanesulfonic Acid as Catalysts. *Synthetic Communications*
487        **2006**, *36* (20), 2957–2961. https://doi.org/10.1080/00397910600773700.
488  (32)  Meng, G.; Zheng, M.-L.; Zheng, A.-Q.; Wang, M.; Shi, J. The Novel Usage of Thiourea Nitrate in Aryl
489        Nitration. *Chinese Chemical Letters* **2014**, *25* (1), 87–89. https://doi.org/10.1016/j.cclet.2013.09.003.
490  (33)  Hegde, G.; Rajkumar, Y. A.; Mei, G. S.; Mahmood, S.; Mandal, U. K.; Sudhakar, A. A. Photoisomerization
491        Behavior of Photochromic Amide-Based Azobenzene Dyes Exhibiting H-Bonding Effect: Synthesis and
492        Characterization. *Korean J. Chem. Eng.* **2016**, *33* (4), 1480–1488. https://doi.org/10.1007/s11814-015-
493        0259-8.
494  (34)  Mathews, M.; Kang, S.; Kumar, S.; Li, Q. Designing Bent-Core Nematogens towards Biaxial Nematic Liquid
495        Crystals. *Liquid Crystals* **2011**, *38* (1), 31–40. https://doi.org/10.1080/02678292.2010.524716.
496  (35)  Stroobants, A.; Lekkerkerker, H. N. W.; Odijk, T. Effect of Electrostatic Interaction on the Liquid Crystal
497        Phase Transition in Solutions of Rodlike Polyelectrolytes. *Macromolecules* **1986**, *19* (8), 2232–2238.

498        https://doi.org/10.1021/ma00162a020.

499   (36)   Meier, G.; Saupe, A. Dielectric Relaxation in Nematic Liquid Crystals. *Molecular Crystals* **1966**, *1* (4), 515–
500        525. https://doi.org/10.1080/15421406608083290.

501   (37)   Vertogen, G.; de Jeu, W. H. *Thermotropic Liquid Crystals, Fundamentals*; Goldanskii, V. I., Schäfer, F. P.,
502        Toennies, J. P., Series Eds.; Springer Series in Chemical Physics; Springer Berlin Heidelberg: Berlin,
503        Heidelberg, 1988; Vol. 45. https://doi.org/10.1007/978-3-642-83133-1.

504   (38)   Gelbart, W. M. Molecular Theory of Nematic Liquid Crystals. *J. Phys. Chem.* **1982**, *86* (22), 4298–4307.
505        https://doi.org/10.1021/j100219a007.

506   (39)   Singh, S. Phase Transitions in Liquid Crystals. *Physics Reports* **2000**, *324* (2–4), 107–269.
507        https://doi.org/10.1016/S0370-1573(99)00049-6.

508   (40)   Israelachvili, J. N. 6 - Van Der Waals Forces. In *Intermolecular and Surface Forces (Third Edition)*;
509        Israelachvili, J. N., Ed.; Academic Press: San Diego, 2011; pp 107–132. https://doi.org/10.1016/B978-0-
510        12-375182-9.10006-5.

511   (41)   Margenau, H.; Kestner, N. *Theory of Intermolecular Forces*, 2nd ed.; Elsevier, 1969.
512        https://doi.org/10.1016/C2013-0-02436-X.

513   (42)   Stone, A. *The Theory of Intermolecular Forces*, 2nd ed.; Oxford University Press, 2013.
514        https://doi.org/10.1093/acprof:oso/9780199672394.001.0001.

515   (43)   Hanwell, M. D.; Curtis, D. E.; Lonie, D. C.; Vandermeersch, T.; Zurek, E.; Hutchison, G. R. Avogadro: An
516        Advanced Semantic Chemical Editor, Visualization, and Analysis Platform. *J Cheminform* **2012**, *4* (1), 17.
517        https://doi.org/10.1186/1758-2946-4-17.

518   (44)   Wang, J.; Wang, W.; Kollman, P. A.; Case, D. A. Automatic Atom Type and Bond Type Perception in
519        Molecular Mechanical Calculations. *Journal of Molecular Graphics and Modelling* **2006**, *25* (2), 247–260.
520        https://doi.org/10.1016/j.jmgm.2005.12.005.

521   (45)   Wang, J.; Wolf, R. M.; Caldwell, J. W.; Kollman, P. A.; Case, D. A. Development and Testing of a General
522        Amber Force Field. *J. Comput. Chem.* **2004**, *25* (9), 1157–1174. https://doi.org/10.1002/jcc.20035.

523   (46)   *Avogadro: An Open-Source Molecular Builder and Visualization Tool. Version 1.2.0*.

524   (47)   Harada, J.; Ogawa, K.; Tomoda, S. Molecular Motion and Conformational Interconversion of
525        Azobenzenes in Crystals as Studied by X-Ray Diffraction. *Acta Crystallogr B Struct Sci* **1997**, *53* (4), 662–
526        672. https://doi.org/10.1107/S0108768197002772.

527   (48)   Biswas, N.; Umapathy, S. Density Functional Calculations of Structures, Vibrational Frequencies, and
528        Normal Modes of *Trans* - and *Cis* -Azobenzene. *J. Phys. Chem. A* **1997**, *101* (30), 5555–5566.
529        https://doi.org/10.1021/jp970312x.

530   (49)   Stewart, J. J. P. Optimization of Parameters for Semiempirical Methods VI: More Modifications to the
531        NDDO Approximations and Re-Optimization of Parameters. *J Mol Model* **2013**, *19* (1), 1–32.
532        https://doi.org/10.1007/s00894-012-1667-x.

533   (50)   Baker, J. An Algorithm for the Location of Transition States. *J. Comput. Chem.* **1986**, *7* (4), 385–395.
534        https://doi.org/10.1002/jcc.540070402.

535   (51)   Kanis, D. R.; Ratner, M. A.; Marks, T. J. Design and Construction of Molecular Assemblies with Large
536        Second-Order Optical Nonlinearities. Quantum Chemical Aspects. *Chem. Rev.* **1994**, *94* (1), 195–242.
537        https://doi.org/10.1021/cr00025a007.

538   (52)   Ladanyi, B. M.; Liang, Y. Q. Interaction-induced Contributions to Polarizability Anisotropy Relaxation in
539        Polar Liquids. *The Journal of Chemical Physics* **1995**, *103* (15), 6325–6332.
540        https://doi.org/10.1063/1.470413.

541   (53)   Kurtz, H. A.; Stewart, J. J. P.; Dieter, K. M. Calculation of the Nonlinear Optical Properties of Molecules.
542        *J. Comput. Chem.* **1990**, *11* (1), 82–87. https://doi.org/10.1002/jcc.540110110.

543   (54)   Skaf, M. S.; Vechi, S. M. Polarizability Anisotropy Relaxation in Pure and Aqueous Dimethylsulfoxide. *The
544        Journal of Chemical Physics* **2003**, *119* (4), 2181–2187. https://doi.org/10.1063/1.1583677.

545   (55)   Smith, S. M.; Markevitch, A. N.; Romanov, D. A.; Li, X.; Levis, R. J.; Schlegel, H. B. Static and Dynamic
546        Polarizabilities of Conjugated Molecules and Their Cations. *J. Phys. Chem. A* **2004**, *108* (50), 11063–
547        11072. https://doi.org/10.1021/jp048864k.

548  (56)  Henderson, P. A.; Seddon, J. M.; Imrie, C. T. Methylene- and Ether-linked Liquid Crystal Dimers II. Effects
549       of Mesogenic Linking Unit and Terminal Chain Length. *Liquid Crystals* **2005**, *32* (11–12), 1499–1513.
550       https://doi.org/10.1080/02678290500284983.
551  (57)  Henderson, P. A.; Niemeyer, O.; Imrie, C. T. Methylene-Linked Liquid Crystal Dimers. *Liquid Crystals* **2001**,
552       *28* (3), 463–472. https://doi.org/10.1080/02678290010007558.
553  (58)  Tschierske, C. Development of Structural Complexity by Liquid-Crystal Self-Assembly. *Angew. Chem. Int.*
554       *Ed.* **2013**, *52* (34), 8828–8878. https://doi.org/10.1002/anie.201300872.
555  (59)  Neubert, M. E.; Carlino, L. T.; Fishel, D. L.; D'sidocky, R. M. The Effect of Terminal Alkyl Chain Length on
556       Mesomorphic Properties of 4-Alkoxyphenyl-4'-Alkylbenzoates. *Molecular Crystals and Liquid Crystals*
557       **1980**, *59* (3–4), 253–272. https://doi.org/10.1080/00268948008071427.
558  (60)  Inglot, K.; Martyński, T.; Bauman, D. Influence of the Alkyl Chain Length of Some Mesogenic Molecules
559       on Their Langmuir Film Formation Ability. *Liquid Crystals* **2006**, *33* (7), 855–864.
560       https://doi.org/10.1080/02678290600733798.
561  (61)  Choi, S.-W.; Izumi, T.; Hoshino, Y.; Takanishi, Y.; Ishikawa, K.; Watanabe, J.; Takezoe, H. Circular-
562       Polarization-Induced Enantiomeric Excess in Liquid Crystals of an Achiral, Bent-Shaped Mesogen. *Angew.*
563       *Chem. Int. Ed.* **2006**, *45* (9), 1382–1385. https://doi.org/10.1002/anie.200503767.
564  (62)  Vera, F.; Tejedor, R. M.; Romero, P.; Barberá, J.; Ros, M. B.; Serrano, J. L.; Sierra, T. Light-Driven
565       Supramolecular Chirality in Propeller-Like Hydrogen-Bonded Complexes That Show Columnar
566       Mesomorphism. *Angew. Chem. Int. Ed.* **2007**, *46* (11), 1873–1877.
567       https://doi.org/10.1002/anie.200603796.
568  (63)  Mathews, M.; Zola, R. S.; Yang, D.; Li, Q. Thermally, Photochemically and Electrically Switchable
569       Reflection Colors from Self-Organized Chiral Bent-Core Liquid Crystals. *J. Mater. Chem.* **2011**, *21* (7),
570       2098–2103. https://doi.org/10.1039/C0JM03479G.
571  (64)  Senyuk, B.; Wonderly, H.; Mathews, M.; Li, Q.; Shiyanovskii, S. V.; Lavrentovich, O. D. Surface Alignment,
572       Anchoring Transitions, Optical Properties, and Topological Defects in the Nematic Phase of Thermotropic
573       Bent-Core Liquid Crystal A131. *Phys. Rev. E* **2010**, *82* (4), 041711.
574       https://doi.org/10.1103/PhysRevE.82.041711.
575  (65)  Fischer, E. Calculation of Photostationary States in Systems A .Dblarw. B When Only A Is Known. *J. Phys.*
576       *Chem.* **1967**, *71* (11), 3704–3706. https://doi.org/10.1021/j100870a063.
577  (66)  Victor, J. G.; Torkelson, J. M. On Measuring the Distribution of Local Free Volume in Glassy Polymers by
578       Photochromic and Fluorescence Techniques. *Macromolecules* **1987**, *20* (9), 2241–2250.
579       https://doi.org/10.1021/ma00175a032.
580  (67)  Morishima, Y.; Tsuji, M.; Kamachi, M.; Hatada, K. Photochromic Isomerization of Azobenzene Moieties
581       Compartmentalized in Hydrophobic Microdomains in a Microphase Structure of Amphiphilic
582       Polyelectrolytes. *Macromolecules* **1992**, *25* (17), 4406–4410. https://doi.org/10.1021/ma00043a025.
583  (68)  Sasaki, T.; Ikeda, T.; Ichimura, K. Photoisomerization and Thermal Isomerization Behavior of Azobenzene
584       Derivatives in Liquid-Crystalline Polymer Matrixes. *Macromolecules* **1993**, *26* (1), 151–154.
585       https://doi.org/10.1021/ma00053a023.
586  (69)  Wang, W.; Wang, M.-Z. Effect of α-Cyclodextrin on the Photoisomerization of Azobenzene Functionalized
587       Hydroxypropyl Methylcellulose in Aqueous Solution. *Polym. Bull.* **2007**, *59* (4), 537–544.
588       https://doi.org/10.1007/s00289-007-0789-2.
589  (70)  Ya, Q.; Dong, X.-Z.; Chen, W.-Q.; Duan, X.-M. The Synthesis of Aminoazobenzenes and the Effect of
590       Intermolecular Hydrogen Bonding on Their Photoisomerization. *Dyes and Pigments* **2008**, *79* (2), 159–
591       165. https://doi.org/10.1016/j.dyepig.2008.02.004.
592  (71)  Fischer, E. Temperature Dependence of Photoisomerization Equilibria. Part I. Azobenzene and the
593       Azonaphthalenes. *J. Am. Chem. Soc.* **1960**, *82* (13), 3249–3252. https://doi.org/10.1021/ja01498a005.
594  (72)  Naito, T.; Horie, K.; Mita, I. Photochemistry in Polymer Solids. 11. The Effects of the Size of Reaction
595       Groups and the Mode of Photoisomerization on Photochromic Reactions in Polycarbonate Film.
596       *Macromolecules* **1991**, *24* (10), 2907–2911. https://doi.org/10.1021/ma00010a042.
597  (73)  Towns, J.; Cockerill, T.; Dahan, M.; Foster, I.; Gaither, K.; Grimshaw, A.; Hazlewood, V.; Lathrop, S.; Lifka,

598        D.; Peterson, G. D.; Roskies, R.; Scott, J. R.; Wilkins-Diehr, N. XSEDE: Accelerating Scientific Discovery.
599        *Comput. Sci. Eng.* **2014**, *16* (5), 62–74. https://doi.org/10.1109/MCSE.2014.80.

600  (74)  Nystrom, N. A.; Levine, M. J.; Roskies, R. Z.; Scott, J. R. Bridges: A Uniquely Flexible HPC Resource for
601        New Communities and Data Analytics. In *Proceedings of the 2015 XSEDE Conference on Scientific
602        Advancements Enabled by Enhanced Cyberinfrastructure - XSEDE '15*; ACM Press: St. Louis, Missouri,
603        2015; pp 1–8. https://doi.org/10.1145/2792745.2792775.

604  (75)  Perri, M. J.; Weber, S. H. Web-Based Job Submission Interface for the GAMESS Computational Chemistry
605        Program. *J. Chem. Educ.* **2014**, *91* (12), 2206–2208. https://doi.org/10.1021/ed5004228.
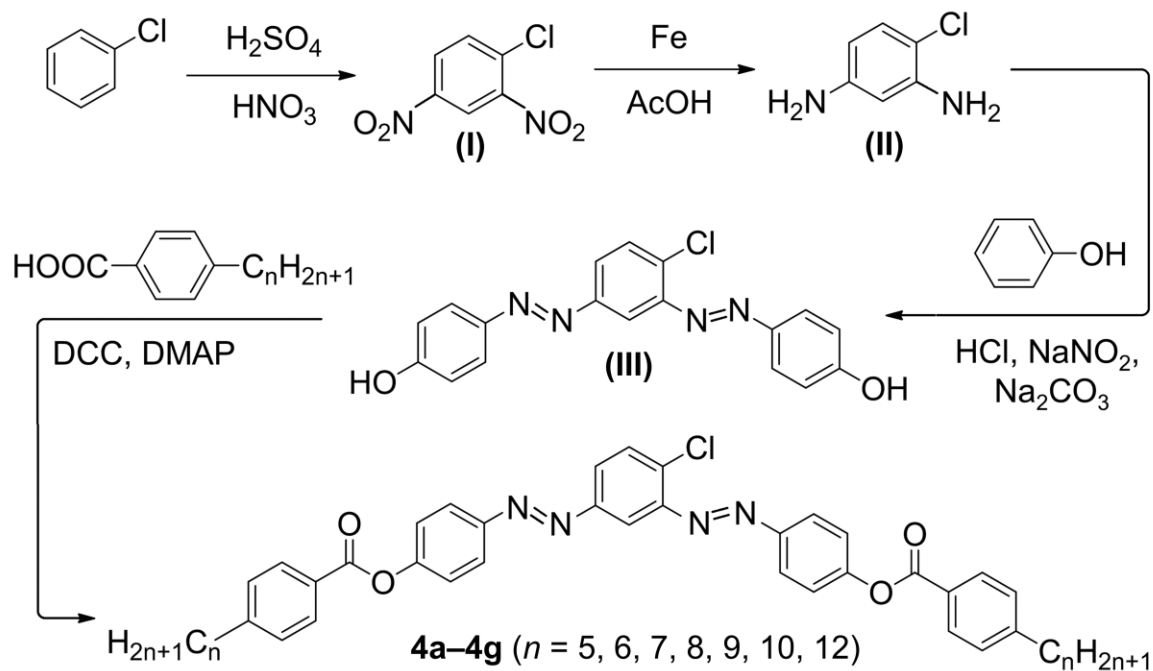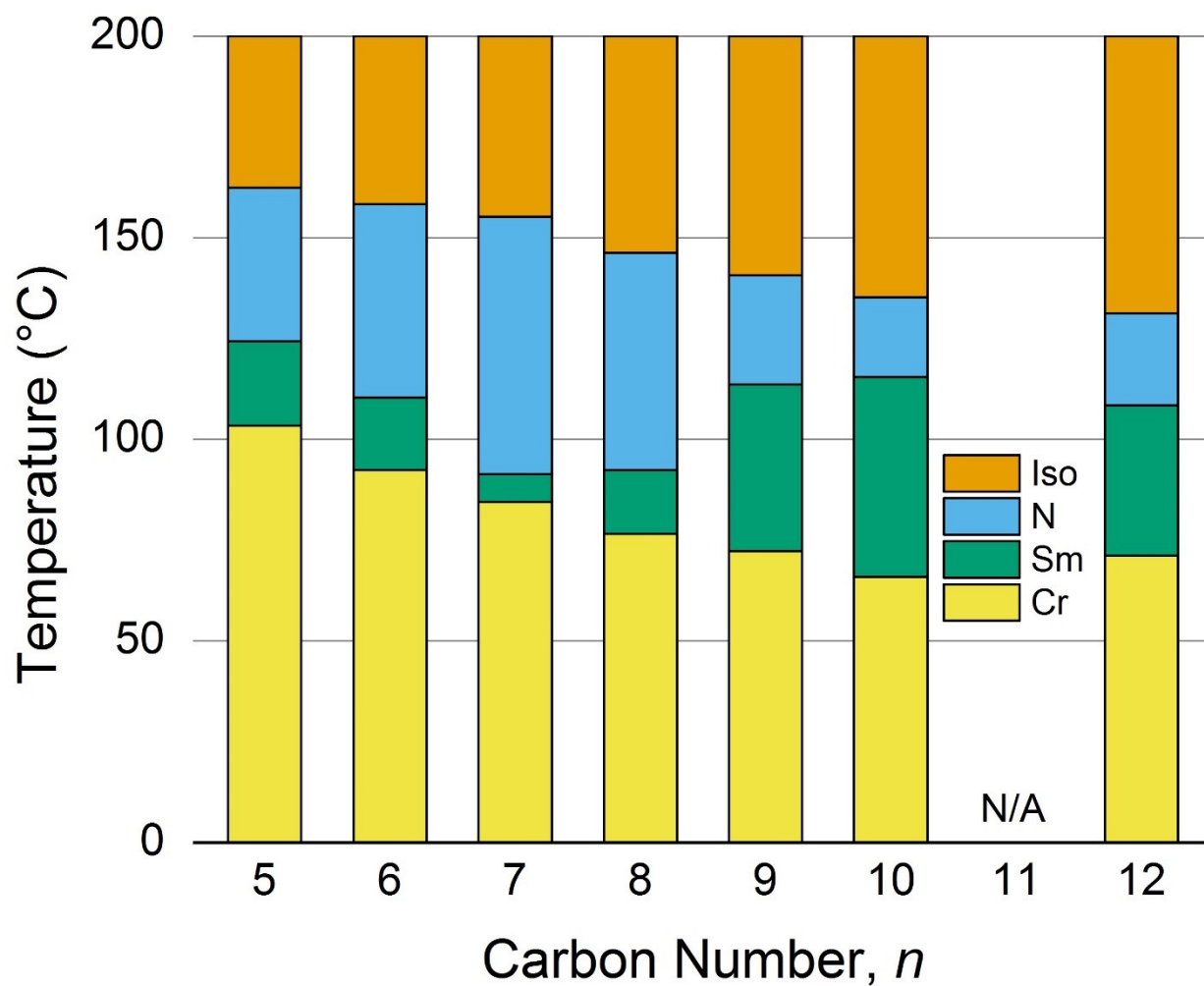
606

607

608

609    Figure 1. Synthesis of 4-chloro-1,3-diazobenzene bent-core liquid crystals **4a–4g**. "*n*" denotes

610    the number of carbon atoms in the terminal alkyl chains.

Figure 2. Phase transition temperatures of compounds **4a–4g**. Yellow, pink, cyan, and grey blocks represent crystalline (Cr) solid, smectic (Sm) phase, nematic (N) phase, and isotropic (Iso) phase, respectively.
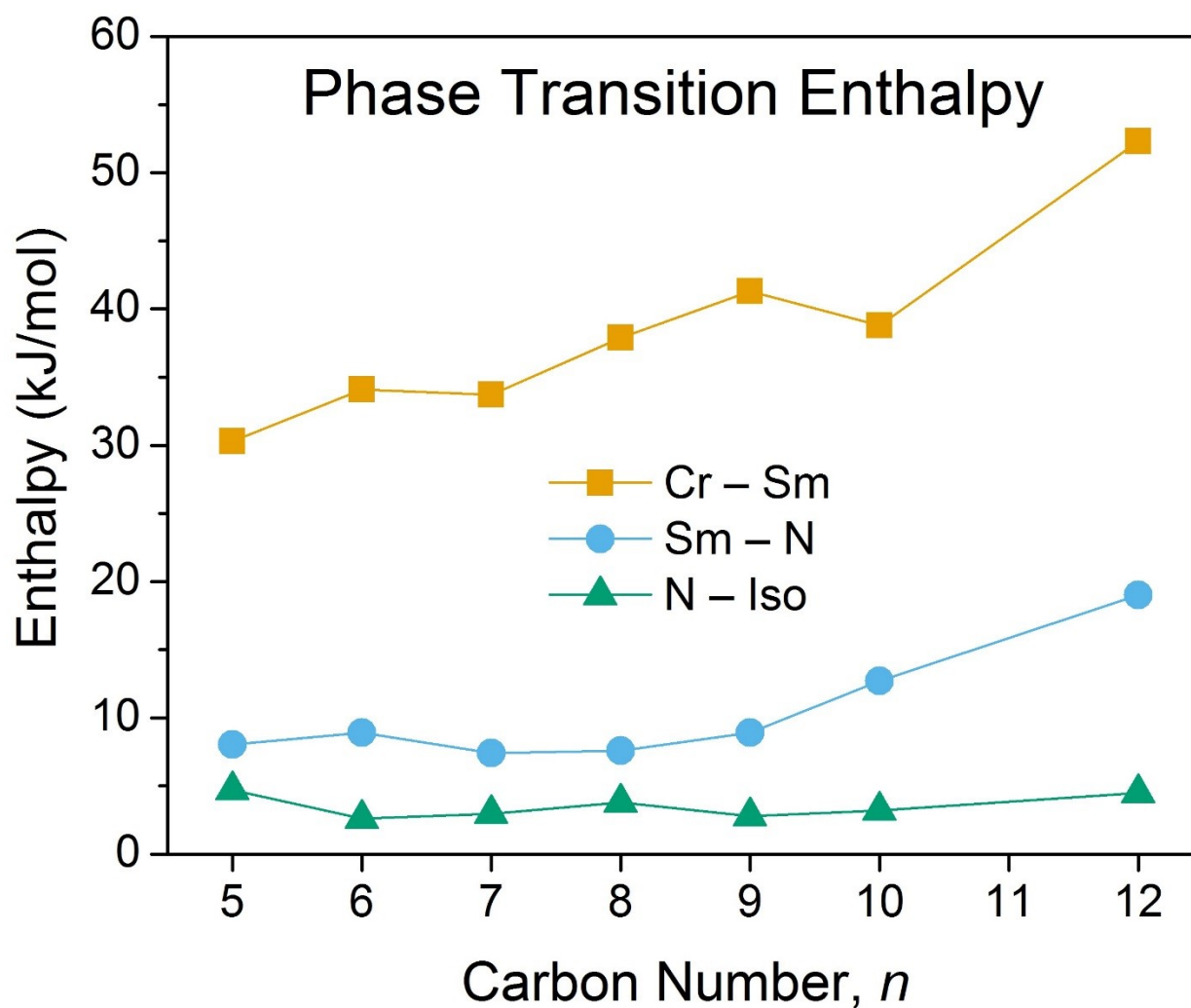
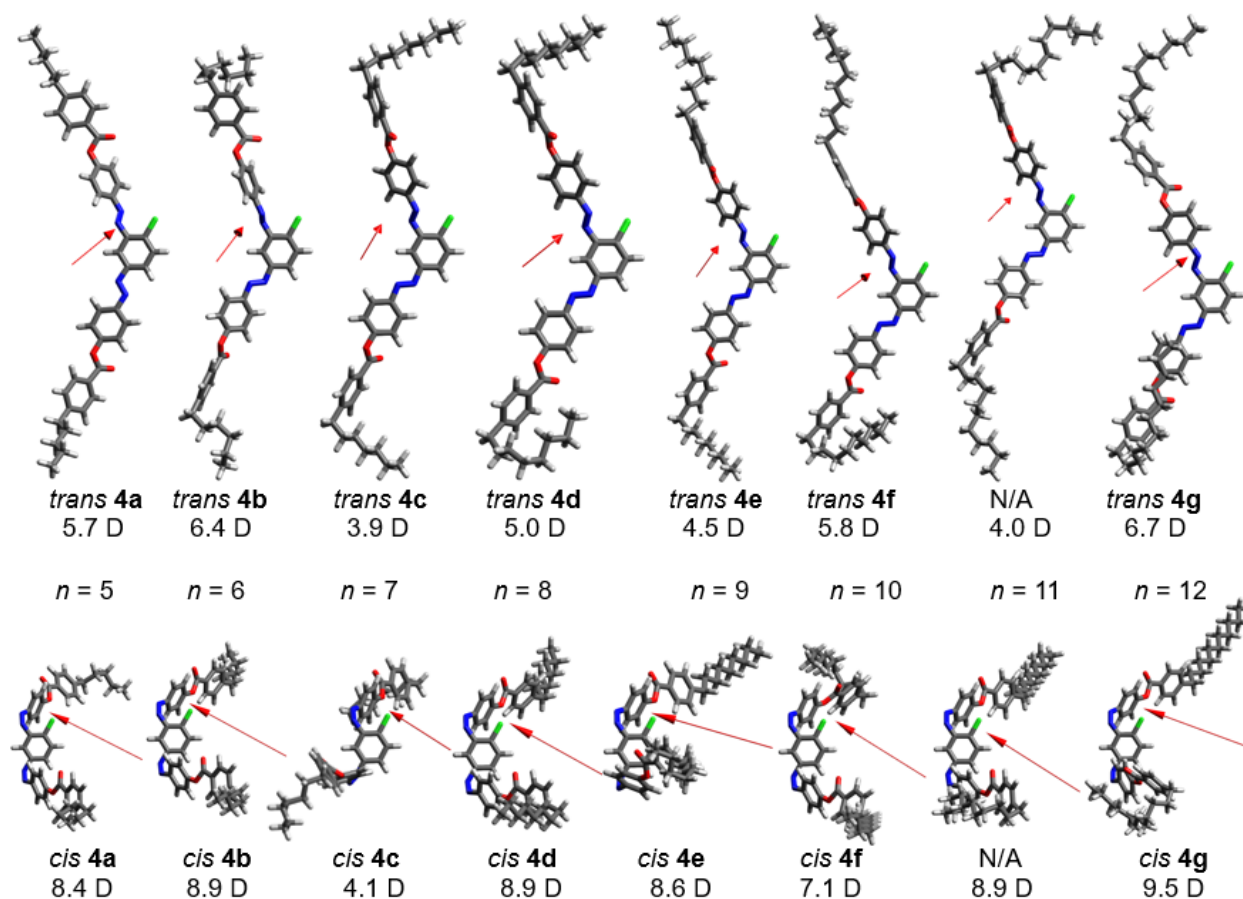Figure 3. Enthalpies for the phase transitions of compounds **4a–4g**.

Figure 4. Molecular structures and dipole orientations of *trans* and *cis* isomers of **4a–4g** in the ground states. The orientations of dipole moment for each type of isomers are generally consistent. The main structural variation within each isomer group is the spatial arrangement of terminal chain. Please note that N/A refers to the compound with n = 11, which is not synthesized in this study. The molecular dipoles were calculated by MOPAC (D: Debye).
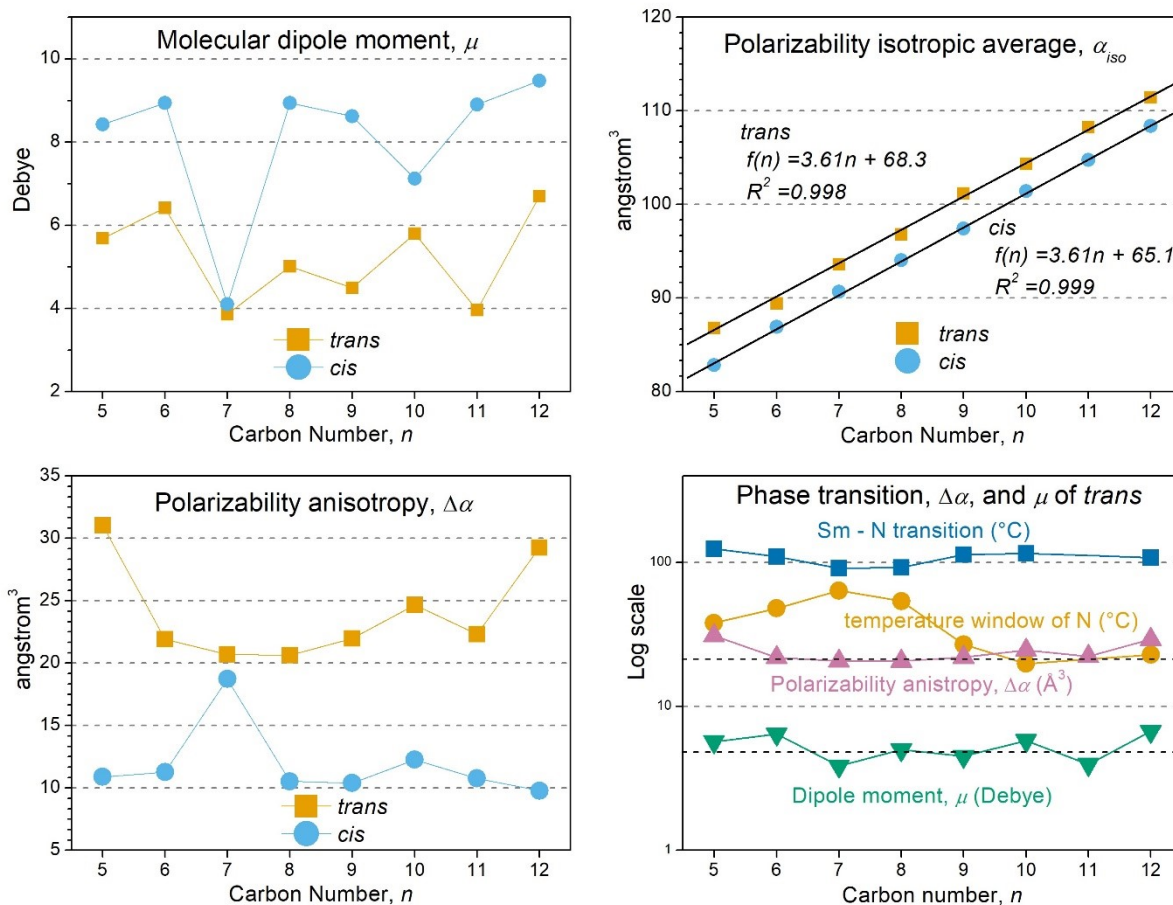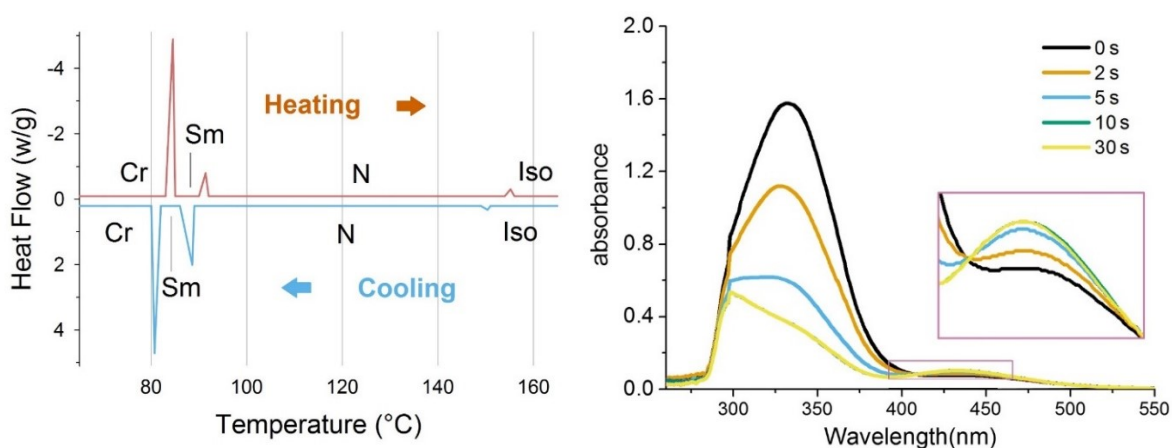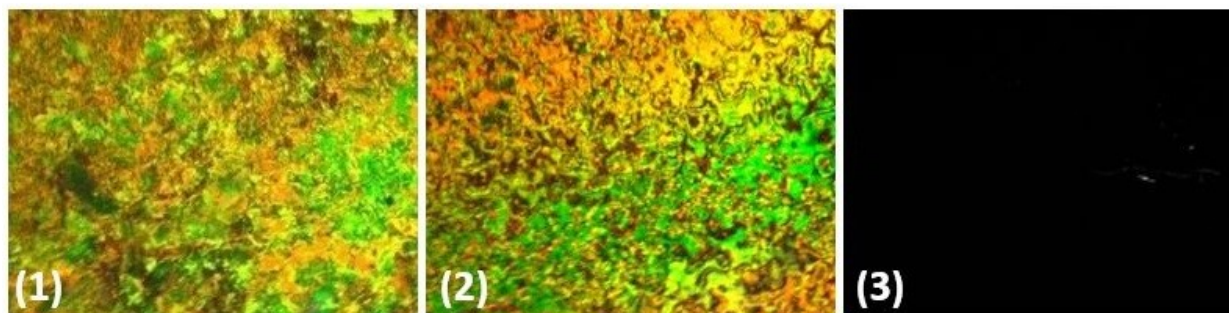
622

Figure 5. Molecular properties of **4a–4g** and their correlation with the Sm – N transition temperature of **4a–4g**. Top left: molecular dipole moments; top right: polarizability; bottom left: polarizability anisotropies; bottom right: comparison between the Sm – N phase transition temperatures, temperature window of nematic phase, polarizability anisotropies, and dipole moments of *trans* isomers of **4a–4g**.
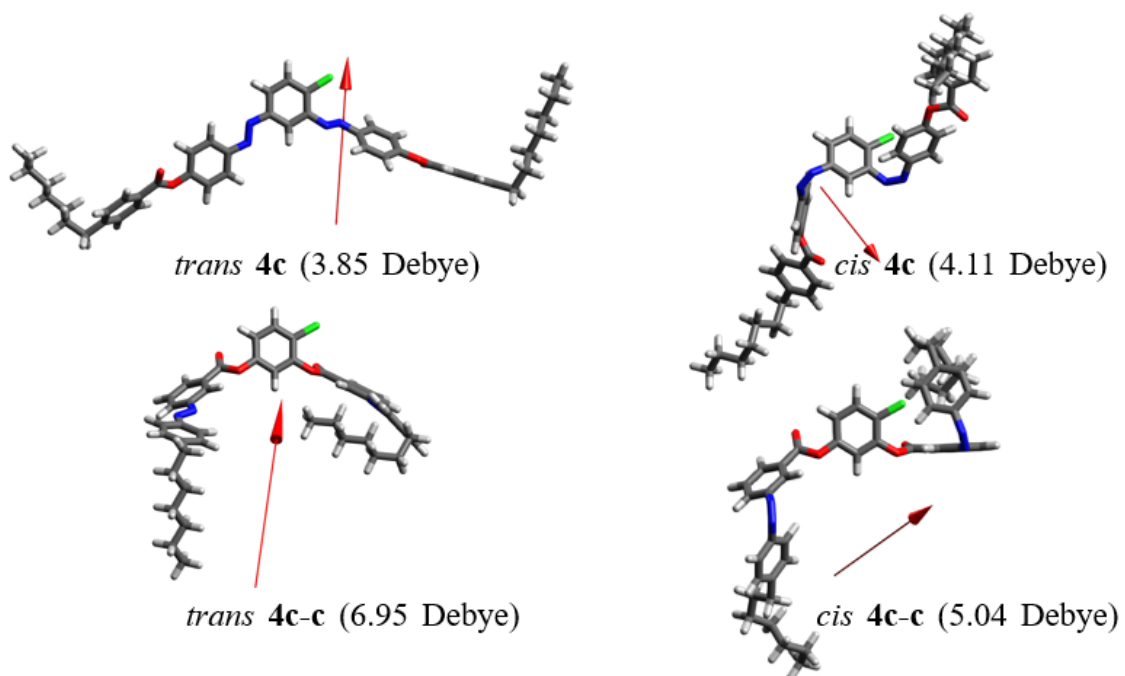
628

629



630



631

Figure 6. Top left: DSC heating and cooling traces of compound **4c**. Top right: UV-Vis spectra of dissolved compound **4c** under 365 nm UV irradiation for 0 s, 2 s, 5 s, 10 s, and 30 s. Bottom 3 insets**:** polarized optical micrograms of compound **4c** under various conditions: (1) smectic textures at 88 °C, (2) nematic textures at 120 °C, and (3) isotropic liquid phase at 155 °C.

636

*trans* **4c** (3.85 Debye)

*cis* **4c** (4.11 Debye)

*trans* **4c-c** (6.95 Debye)

*cis* **4c-c** (5.04 Debye)

637

638  Figure 7. Molecular structures and dipole moments of isomers of compound **4c** and its counterpart

639  **4c-c** at the ground states. Red arrows represent the direction of dipole moment.

640

641 Table 1. Phase transition temperatures of compound **4a–4g**. "*n*" denotes the carbon number in the
642 terminal alkyl chain; "Cr – Sm" phase transition from crystalline phase; "Sm" the smectic phase;
643 "N" the nematic phase; "Iso" the isotropic liquid; "T" the phase transition temperature in °C; "△H"
644 the reaction enthalpy in kJ/mol; "$\Delta T_{LC}$" the temperature window of liquid crystal phase in °C;
645 "$\Delta T_N$" the temperature window of nematic phase in °C ($\Delta T_N = |T_{N-Iso} - T_{Sm-N}|$ ).

| Compound | *n* | Cr – Sm | | Sm – N | | N – Iso | | $\Delta T_{LC}$ (°C) | $\Delta T_N$ (°C) |
|---|---|---|---|---|---|---|---|---|---|
| | | T (°C) | △H (kJ/mol) | T (°C) | △H (kJ/mol) | T (°C) | △H (kJ/mol) | | |
| **4a** | 5 | 103.37 | 30.3 | 124.36 | 8.05 | 162.36 | 4.7 | 58.99 | 38.00 |
| **4b** | 6 | 92.38 | 34.1 | 110.36 | 8.9 | 158.36 | 2.6 | 65.98 | 48.00 |
| **4c** | 7 | 84.52 | 33.7 | 91.36 | 7.4 | 155.2 | 2.95 | 70.68 | 63.84 |
| **4d** | 8 | 76.56 | 37.9 | 92.35 | 7.6 | 146.23 | 3.8 | 69.67 | 53.88 |
| **4e** | 9 | 72.35 | 41.3 | 113.65 | 8.9 | 140.62 | 2.8 | 68.27 | 26.97 |
| **4f** | 10 | 65.92 | 38.8 | 115.46 | 12.7 | 135.26 | 3.2 | 69.34 | 19.80 |
| **4g** | 12 | 71.2 | 52.3 | 108.36 | 19 | 131.26 | 4.5 | 60.06 | 22.90 |

646

647

648    Table 2. Molecular dipole moments ($\mu$), polarizabilities ($\alpha$), and polarizability anisotropies ($\Delta\alpha$) of
649    compound **4a–4g** calculated by MOPAC. "*n*" denotes the number of carbon atoms in each terminal
650    alkyl chain.

| Compound | *n* | *trans* | | | *cis* | | |
|:---:|:---:|:---:|:---:|:---:|:---:|:---:|:---:|
| | | $\mu$ (D) | $\alpha$ (Å$^3$) | $\Delta\alpha$ (Å$^3$) | $\mu$ (D) | $\alpha$ (Å$^3$) | $\Delta\alpha$ (Å$^3$) |
| **4a** | 5 | 5.689 | 86.8 | 31.0 | 8.424 | 82.9 | 10.9 |
| **4b** | 6 | 6.419 | 89.4 | 21.9 | 8.938 | 86.9 | 11.3 |
| **4c** | 7 | 3.854 | 93.6 | 20.7 | 4.107 | 90.7 | 18.7 |
| **4d** | 8 | 5.010 | 96.8 | 20.6 | 8.937 | 94.0 | 10.5 |
| **4e** | 9 | 4.498 | 101.2 | 22.0 | 8.618 | 97.4 | 10.4 |
| **4f** | 10 | 5.795 | 104.3 | 24.7 | 7.119 | 101.4 | 12.3 |
| **N/A** | 11 | 3.964 | 108.3 | 22.3 | 8.905 | 104.8 | 10.8 |
| **4g** | 12 | 6.700 | 111.4 | 29.2 | 9.472 | 108.4 | 9.8 |

651

652     Table 3. Comparison of molecular properties between **4c** and its diester counterpart **4c-c.**

|  | $\mu$ (Debye) | $\alpha$ (Å$^3$) | $\Delta\alpha$ (Å$^3$) | $\mu$ (Debye, DFT) |
|---|---|---|---|---|
| *trans* **4c** | 3.854 | 93.6 | 20.7 | 3.733155 |
| *trans* **4c-c** | 6.951 | 92.0 | 16.5 | 6.562452 |
| *cis* **4c** | 4.107 | 90.7 | 18.7 | 4.028691 |
| *cis* **4c-c** | 5.038 | 89.0 | 7.5 | 3.499278 |

653

654